Journal of ELECTRICAL ENGINEERING, VOL 74(2023), NO2, 75–84

sciendo

PAPERS

Accuracy of scanning interrogation of FBG sensors

František Urban Jr[1], Radek Helán[2], František Urban Sr[3]

Progress in the fibre optic technology spurred the development of optical fibre-based sensors. A successful fibre optics-based element for sensorial systems is fibre Bragg grating. It allows to read the measured value by the spectral shift of light, which is the variable with a good potential for accurate measurement. Various types of the interrogation of the light spectrum reflected from the measuring grating are discussed in this article and the work concentrates on the spectrum scanning that gives the good chances to diminish measuring errors by a proper choice of parameters. The focal point is the accuracy of establishing the correct value of the maximum reflectance wavelength. The significance of the noise in the photoelectric scanning signal for the measuring accuracy is analysed and the crucial factor is found in the minimizing the reflectance spectral width of the measuring grating and using the spectrum of the scanning light with the same or smaller spectral width. An important aspect is the relation of the maximal reflectance and the wavelength width of the measuring grating reflectance spectrum. The article also shows the potentiality of the apodized gratings for improving the scanning interrogation. A specific index apodization profile was analysed and its advantages are discussed.

K e y w o r d s: fibre Bragg grating, interrogation, reflectance spectrum linewidth, apodized grating

1 Introduction

Optical fibre-based sensors began finding their application in measuring the values of physical quantities shortly after the optical fibers obtained the prime position in telecommunication data transfer [1-8]. Fibre Bragg gratings (FBGs) were found to be specific wavelength selective fibre elements with great prospects in optical signal filtering. They were soon investigated with objective to use their facilities in sensing, first for scientific, then for commercial applications [9-16].

Fibre Bragg gratings are elements formed in the core of a single-mode optical fibre (SMF) by variation of its core refractive index. Periodical or quasi-periodical changes of the fibre core refractive index create a longitudinal dispersive structure that reflects light in a narrow range of wavelengths around the central Bragg resonance wavelength λ_B [17-20]. The behaviour of the structure can be represented by a selective optical filter in which the Bragg wavelength is given by

$$2\Lambda_G = \frac{s\lambda_B}{n_{eff}}, \tag{1}$$

where, s - is an integer, Bragg order; Λ_G - is the Bragg period of the refractive index; n_{eff} - is the effective refractive index of the waveguide with the grating, [17].

In the same way, the transmitted light lacks the part of the spectrum reflected from the grating. All physical factors that can alter either the period Λ_G or the effective index n_{eff} of the structure can influence the reflected spectrum of the grating, see Fig. 1. Amongst the most used are temperature of the fibre, strains, twists of the fibre, fibre bends. The spectrum changes induced by the physical agents are mostly expressed by the wavelength shift of the spectral reflectance maximum of the biased

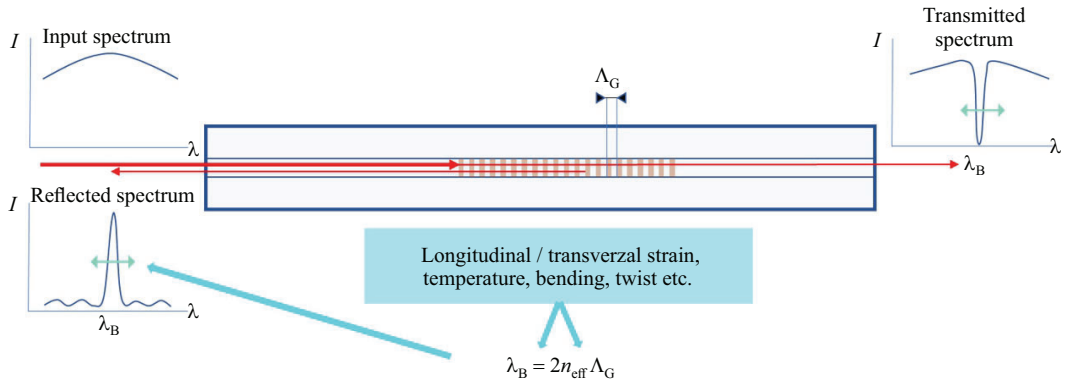

Fig. 1. Fibre Bragg grating sensing principle

[1] Brno University of Technology, FEEC, Department of Teleinformatics, [2] Network Group s.r.o., Department of Special Fibre Optics, [3] Brno University of Technology, FEEC, Department of Microelectronics, urban@proficomms.cz

https://doi.org/10.2478/jee-2023-0010, Print (till 2015) ISSN 1335-3632, On-line ISSN 1339-309X

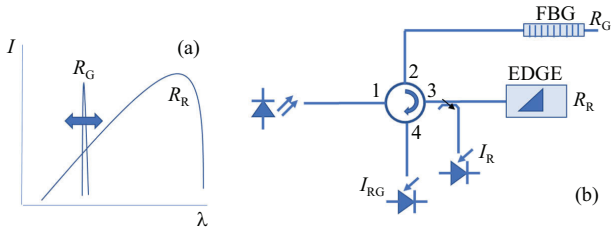

Fig. 2. FBG interrogation by edge filter overlaying: (a) – edge filter reflectance spectrum r_R and FBG reflectance spectrum r_G overlaying, (b) – evaluation schematics with I_R being the reference signal of r_G spectrum, and I_{RG} the detected signal of overlaying the r_R and r_G spectra

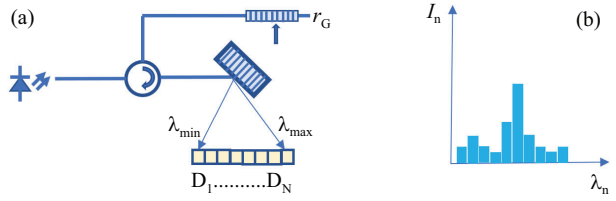

Fig. 3. Interrogation of the FBG by the spectral decompozition, (a) – principal scheme, (b) – signals at the detector array

grating. The wavelength shift that bears the sensing information is highly resistant to the disturbances in the measurement and it is mostly very accurately related to the measured physical value.

The interrogation of the fibre Bragg grating based sensorial elements is the task to evaluate the spectral shift of the reflectance (or transfer) spectra of the grating corresponding to the measured value. This task can be solved in a number of ways, each one giving a specific compromise between the accuracy and the data acquisition frequency [21,22].

A generally accepted fact is that direct spectral wavelength measurements belong to the most accurate measurements ever. On the other hand, the wavelength measurements are not the fastest ones, by far. Favourite methods of grating wavelength evaluation are those which convert the wavelength shift of the grating spectrum to the intensity of the reflected/transmitted light for further direct detection. The overlaying of the measured spectrum with the triangle-like spectrum of the edge filter can serve as a representative of these methods. In this method, the radiation of the broadband light source like a superluminiscent light emitting diode (SLED) or amplified spontaineous emission (ASE) based source is lounched to arm 1 of the fiber circulator, see Fig. 2. Light then propagates to arm 2 where it is reflected from the measuring FBG. The reflected light further goes to arm 3 of the circulator where it is reflected from the reference edge filter that converts the spectral position of the reflecting maximum of the FBG to the relevant intensity level. This combined reflection is then detected and converted to the electrical signal in arm 4 of the circulator. To diminish the influence of the intensity fluctuations and spectral uneveness of the optical source and the influence of loss instabilities in the optical network, the detected signal I_{RG} is referenced by signal I_R, the detected sample of the reflection from the sensing FBG. Having the capacity of working very fast, this method suffers from low accuracy, nonlinearity and time instability. Instabilities and noises of the optical sources and detectors can seldom allow the accuracy of this method to reach the level of 10^{-3} of the measured range that leads to the wavelength shift resolution $\Delta\lambda_G$ not better than 10 pm.

Opposite situation is met with the measurement of the FBG spectrum wavelength shift by the decomposition of the spectral components of the measured light and their parallel detection and evaluation, see Fig. 3. Here, the light from the broadband source goes to arm 1 of the circulator, then from arm 2 to the measuring FBG where it is reflected and through arm 3 comes to the bulk diffractive element that reflects each spectral component of light in a different angle. The diffractive element works in the measuring range $\Delta\lambda_m = \lambda_{max} - \lambda_{min}$, going from the shortest measured wavelength λ_{min} to the longest measured wavelength λ_{max}. The separated spectral components with wavelengths λ_n in the measuring range $\Delta\lambda_m$ reach individual cells of the CCD, CID or diode detector array D1-DN, where they are converted to electrical signals and evaluated.

Wavelength resolution of the FBG interroation in this case depends on the tetector array size, often the achieved resolution goes down to several pm. The implementations of this method are usually very stabile, although with not very fast response. As the most common spectral

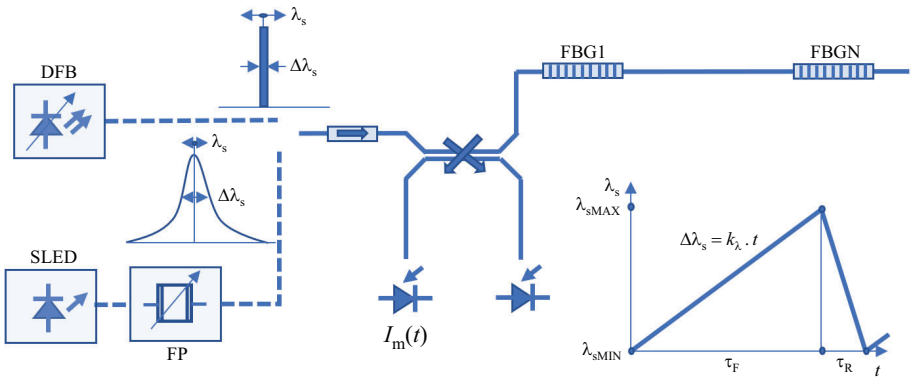

Fig. 4. Scaning interrogation scheme

range used in FBG sensing is the O band 1310 nm, where fibres are still only moderately sensitive to the bending losses. However the necessary GaInP detector arrays are representing considerable cost rising factor here. With the pixel count of $N = 2048$ px and measuring range $\Delta\lambda_{\mathrm{m}}$ for one FBG being around 3 nm, we can expect the spectral resolution of this method

$$\Delta\lambda_{\mathrm{G}} = \frac{\Delta\lambda_{\mathrm{m}}}{N} = 1 \text{ to } 2 \text{ pm}. \tag{2}$$

For the case of more simultaneously interrogated FBG sensors in the wavelength multiplex, the range of the detector pixels is divided to the sub-ranges for the individual gratings resulting in worsenned resolution $\Delta\lambda_{\mathrm{GM}}$ proportionally to the number M of the simultaneously interrogated gratings

$$\Delta\lambda_{\mathrm{GM}} = M\Delta\lambda_{\mathrm{G}}\,. \tag{3}$$

The limited number N of the detector pixels in the detector array limits the spectral measurement resolution. That factor can be avoided by means of spectral scanning.

2 Spectral scanning

This interrogation method is based on the source of tuneable light with a narrow-band spectrum. As shown by the scheme in Fig. 4., the light source is connected to the fibre isolator and a 50:50 symmetrical coupler. That splits the incident light to two arms, the arm with the interrogated series of gratings and the arm with the reference detector. After the light is partially reflected from the sensorial FBGs, it is forwarded back to the coupler. The reflected light then reaches the measuring detector. The signal of the measuring detector is then normalized to the reference detector received value. The light tuning follows the linear ramp function as shown in Fig. 4. The central wavelength of the tuned light λ_{s} goes linearly in time from the $\lambda_{\mathrm{s,min}}$ to the $\lambda_{\mathrm{s,max}}$ value. The light power incident to the signal detector reaches the maximum when the scanning light wavelength λ_{s} crosses the wavelength of the maximal reflectance of the measuring FBG. The time of that maximum is then located from the signal of the measuring detector and recalculated to the wavelength value of the maximal reflectance of the sensorial grating. Typically, one can see the two types of spectrum scanning. Very often we see the first type that uses an ultranarrow band tunable optical source, often a distributed feedback-based laser diode (DFB-LD), offering the spectral bandwidth in a -20 dB drop, typically $\Delta f_{20} < 100$ MHz, $\Delta\lambda_{20} = 0.8$ pm. The drawback of this type of scanning is the low tuning range $\lambda_{\mathrm{s,min}}$ to $\lambda_{\mathrm{s,max}}$ and the low speed of the laser diode tuning k_λ. The cost saving DFBs, standard telecom grade ones, provide the modest tuning range of 10 nm in the O or C band and not more than $k_\lambda = 10$ nm/s tuning speed. The second type of scanning uses the stable broadband light source (for instance a superluminescent light emitting diode, SLED) filtered by a tunable narrowband Fabry-Perot filter to scan the FBG spectrum. This combination gives the scanning frequency to several hundreds Hz and the tuning range up to 100 nm. This situation allows connecting more than 20 FBGs to the scanning interrogator in series. On the other side, the tunable FP filters work with a much wider spectrum line than what one can get with DFBs. The typical value of the FP filter full width half maximum linewidth (FWHM) is $\Delta\lambda_{\mathrm{sF}} \cong 60$ pm, hence $\Delta\lambda_{20} \cong \Delta\lambda_{\mathrm{sF}}/0.603 = 99.5$ pm, [22].

The photoelectric signal $I_{\mathrm{m}}(t)$ of the measuring detector corresponds to the reflectance spectrum of the sensing FBG. However, the time dependence of the signal $I_{\mathrm{m}}(t)$ is not a fully linear copy of the FBG spectrum. In practice it represents a corelation function of the spectral reflectance of FBG and the scanning light spectrum and is expressed as

$$I_{\mathrm{m}}(t) = \int_{\lambda_{\min}}^{\lambda_{\max}} r_{\mathrm{g}}(\lambda) I_{\mathrm{s}}\Big(\lambda - \Delta\lambda_{\mathrm{s}}(t)\Big)\mathrm{d}\lambda, \tag{4}$$

where $\Delta\lambda_{\mathrm{s}}(t) = k_\lambda t$ is the wavelength shift of the scanning spectrum, $r_{\mathrm{g}}(\lambda)$ is the spectral light reflectance of FBG, and $I_{\mathrm{s}}(\lambda)$ is the scanning light spectral intensity.

The main peak of the time signal received at the measuring detector has its maximum positioned at the instance of coincidence of FBG spectral reflectivity maximum and tunable source spectrum maximum provided the two spectra are near to symmetrical with respect to their maxima. The full width at half-maximum value of the time signal peak is generally different from the original FBG spectrum. It can be widened or narrowed depending on the scanning spectrum linewidth. Figure 5. shows some examples of scanning. We can compare the time signals $I_{\mathrm{m}}(t)$ represented in the wavelength domain (green lines in the spectral charts) with the shape of the original grating reflectance spectrum (blue lines in the spectral charts). The presented cases use the scanning spectrum FWHM linewidth narrower (30 pm), equal (82.5 pm) and wider (120 pm) than the FWHM linewidth of the interrogated grating. The interrogated grating parameters are as follows: grating type is uniform (design No. 10-82) with the amplitude of the refractive index modulation $\Delta n = 1.25 \times 10^{-4}$, grating length $L = 11$ mm, grating reflectance maximum $r_{\max} = 85.6\%$, grating reflectance FWHM linewidth $\Delta\lambda_{\mathrm{GF}} = 82.46$ pm. The graphs in Fig. 5 demonstrate the changes of the scanned spectra, where the FWHM linewidth and the shape of the top of the spectrum are important affected parameters. Both of them are significant for the noise influence in detecting the wavelength position of the grating reflectance spectral maximum. The key issue of the FBG spectral shift interrogation is the accuracy of the detection of the wavelength position of maximum grating reflectance. This accuracy is established by the resolution of the wavelength measurement $\Delta\lambda_{\mathrm{G}}$, which is determined

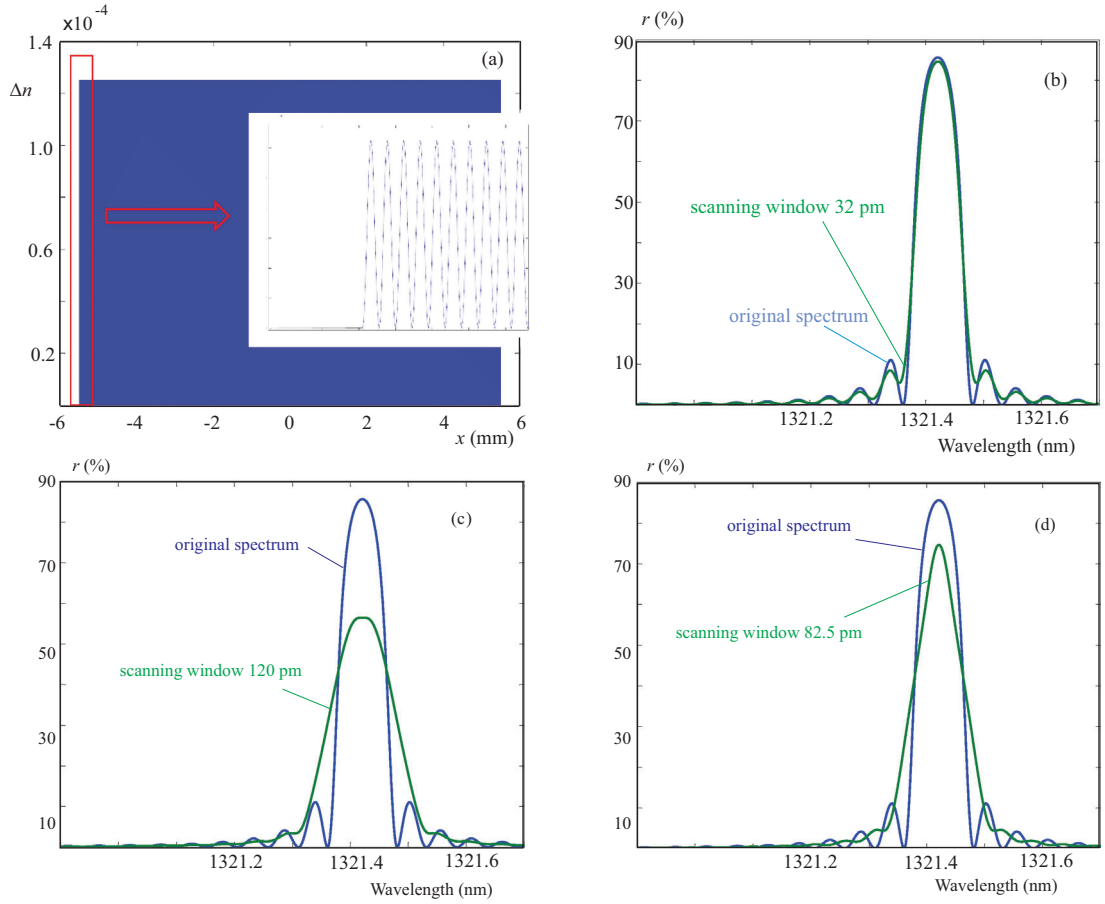

Fig. 5. Uniform grating design No. 10-82, (a) – refractive index profile; original and scanned spectrum of the grating with (b) – $\Delta\lambda_{sF} = 30$ pm, (c) – 82.5 pm, and (d) – 120 pm

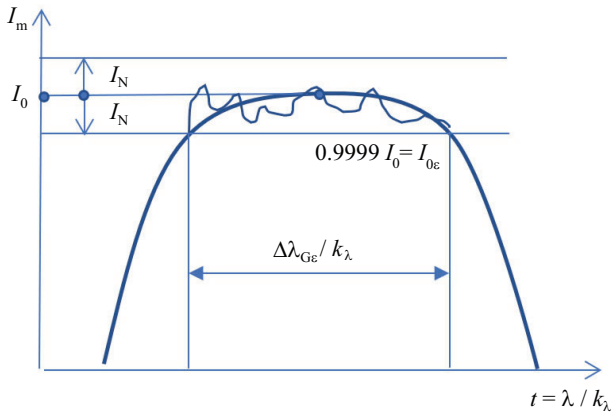

Fig. 6. The effect of superimposed noise to the location of reflectance maximum

by the scanning period T_{SC}, the sampling period T_{SA} of signal $I_m(t)$, and the scanning wavelength range, [22]

$$\Delta\lambda_G = (\lambda_{s,max} - \lambda_{s,min})\frac{T_{SA}}{T_{SC}} \leq 0.01\,\text{pm}. \qquad (5)$$

Provided the tuned light wavelength shift is a linear time function in the range of $\lambda_{s,max} - \lambda_{s,min}$, as shown by the graph in Fig. 4 and the sampling period is short, the wavelength resolution can be very small.

Two fundamental factors influence the detection of the wavelength position of the maximum grating reflectance. The first one is the linewidth of the central maximum of the reflectance spectrum of the grating, the second one is the noise superimposed on the time signal $I_m(t)$ at the measuring detector circuit.

3 Noise

The time signal $I_m(t)$ detecting the time evolution of the reflexed power from the scanned grating is distorted by the superimposed noise I_N. It aggravates the correct determination of the wavelength position of the scanned grating reflexivity maximum. The photodetector circuits of the scanning system bring several sources of noise that affect the signal. The most important ones are the dark current detector noise I_{DN}, the detector shot noise I_{SH} and the thermal noise of the detector load circuit I_{TH}. In our case, in sensing networks, we can see relatively high levels of the received optical signal with respect to the usual levels seen in the fiber data communication systems. This implies the dominating noise source is the detector shot noise I_{SH}. The typical example with the most common values of the receiver bandwidth $W_B = 1$ MHz, transimpedance load resistor $R_C = 50\,\text{k}\Omega$, detector dark current $I_D = 1$ nA, detector photoelectric current for the 100% grating reflectance $I_0 = 50\,\mu$A (corresponding to

the received power in order of $50\,\mu$W) shows these RMS values of noise currents, [22]

$$\begin{aligned} I_{\mathrm{DN}} &= \sqrt{2eI_{\mathrm{D}}W_{\mathrm{B}}} = 30\,\mathrm{pA}, \\ I_{\mathrm{TH}} &= \sqrt{4kTW_{\mathrm{B}}/R_{\mathrm{C}}} = 0.57\,\mathrm{nA}, \\ I_{\mathrm{SH}} &= \sqrt{2eI_0W_{\mathrm{B}}} = 4\,\mathrm{nA} \end{aligned} \tag{6}$$

therefore $I_N \cong I_{\mathrm{SH}} = 4\,\mathrm{nA}$. So, we get the signal to noise ratio at the photoelectric receiver in the form

$$\frac{I_{\mathrm{S}}}{I_{\mathrm{N}}} = \frac{I_0 r_{\max}}{\sqrt{2eI_0 r_{\max}W_{\mathrm{B}}}} = K\sqrt{r_{\max}} \cong 10^4. \tag{7}$$

Here, the grating factor is represented by the grating reflectance $r_{\max}$. The signal-to-noise ratio therefore linearly grows with the increase of the square root of the grating reflectance $\sqrt{r_{\max}}$. Besides, there is another conclusion of our application example, showing that the noise root mean square I_{N} of the superimposed noise on the detector time signal $I_{\mathrm{m}}(t)$ is in the order of 10^{-4} of the signal current $I_{\mathrm{m}}(t)$ at the spectral top of the grating reflexivity. This situation is shown in Fig. 6.

The superimposed noise I_{N} gives the origin of rising errors in determining the time and wavelength position of the time signal $I_{\mathrm{m}}(t)$ maximum and hereby the errors in determining the reflectance spectral maximum.

In Fig. 6 one can see that the detected maximum in the signal, composed of the photoelectric response $I_{\mathrm{m}}(t)$ to the light reflected from the scanned grating and the superimposed noise current with the root mean square value $I_{\mathrm{N}} = 10^{-4}I_0$, will be found with high probability in the time interval $\Delta\lambda_{\mathrm{G}\epsilon}/k_\lambda$ or in the relevant wavelength range $\Delta\lambda_{\mathrm{G}\epsilon}$.

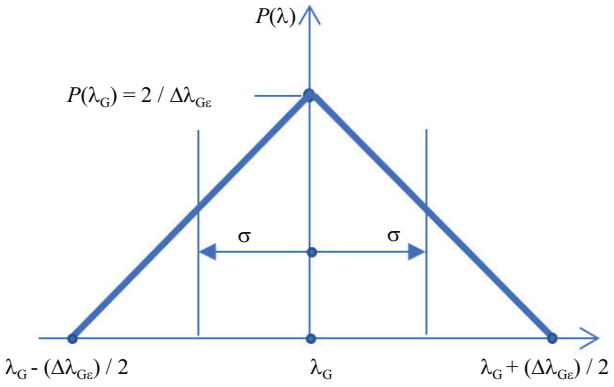

Fig. 7. Probability rate of the position of maximum in $I_{\mathrm{m}}(t)$ signal

We will call that important interval $\Delta\lambda_{\mathrm{G}\epsilon}$ the grating noise linewidth. Probability rate $P(\lambda_{\mathrm{G}})$ of the position of the maximum in $I_{\mathrm{m}}(t)$ signal with the superimposed noise I_{N}, is not constant in the grating noise linewidth $\Delta\lambda_{\mathrm{G}\epsilon}$. The probability rate $P(\lambda_{\mathrm{G}})$ can be, with insignificant simplification, represented by the ramp function, as shown in Fig. 7. Here we can see that the highest probability of finding the grating reflectance maximum is in the central position $\lambda = \lambda_{\mathrm{G}}$. The root mean square deviation of the location of detected maximum from its central position, in other words the mean error of the wavelength position of the maximum reflectance measurement, is

$$\sigma = \frac{\Delta\lambda_{\mathrm{G}\epsilon}}{2\sqrt{6}}. \tag{8}$$

Regarding the fact that in most cases of uniform gratings the spectral reflectance $r(\lambda)$ has the form

$$r(\lambda) = r_{\max}\left(\frac{\sin\kappa}{\kappa}\right)^2, \quad \kappa = \frac{2\pi(\lambda - \lambda_{\mathrm{G}})}{\Delta\lambda_{\mathrm{G20}}}, \tag{9}$$

one obtains

$$\begin{aligned} \Delta\lambda_{\mathrm{G}\epsilon} &\cong 0.022\Delta\lambda_{\mathrm{GF}}, \\ \lambda_{\mathrm{GF}} &\cong 0.603\Delta\lambda_{\mathrm{G20}}, \end{aligned} \tag{10}$$

where $\Delta\lambda_{\mathrm{G20}}$ represents the spectral linewidth at -20dB drop below the maximum.

Therefore, a further important factor in the grating design affecting the accuracy of the maximum reflectance position measurement is the grating noise linewidth $\Delta\lambda_{\mathrm{G}\epsilon}$ that is related to the grating reflectance spectral linewidth in the half maximum $\Delta\lambda_{\mathrm{GF}}$. As the parameters $\sqrt{r_{\max}}$ and $\Delta\lambda_{\mathrm{GF}}$ are not independent, we define the grating quality factor

$$Q_{\mathrm{G}} = \frac{r_{\max}}{\Delta\lambda_{\mathrm{GF}}} \quad (-, \%, \mathrm{nm}). \tag{11}$$

This assesses the grating design from the point of accurate scanning interrogation.

4 Grating design

The grating parameters like maximum reflectance $r_{\max}$ and the reflectance full width half maximum spectral linewidth $\Delta\lambda_{\mathrm{GF}}$ are mutually coupled quantities. The physical length of the grating in the fibre is the main factor influencing these two parameters. The length of the fibre grating for the sensorial use is often limited or determined by the specific application. Frequently, the designer meets the request for a limited grating structure length due to the needs to limit the subsequent troubles in proper fixing or protecting the fibre sensorial structure. The design simulation results shown in the 3D graphs of Figs. 8(a) and (b) depict the relations of the grating full width at half maximum linewidth Δ_{GF} and the grating noise linewidth $\Delta\lambda_{\mathrm{G}\epsilon}$ to the length L of the gratings and to the grating maximal reflectance $r_{\max}$. The graphs in Figs. 8(c) to (e) give the guidance for the optimal choice of $r_{\max}$, and the achievable values of the grating noise linewidths for various typical lengths of the uniform grating used in sensorial applications. Further, Fig. 8(f)

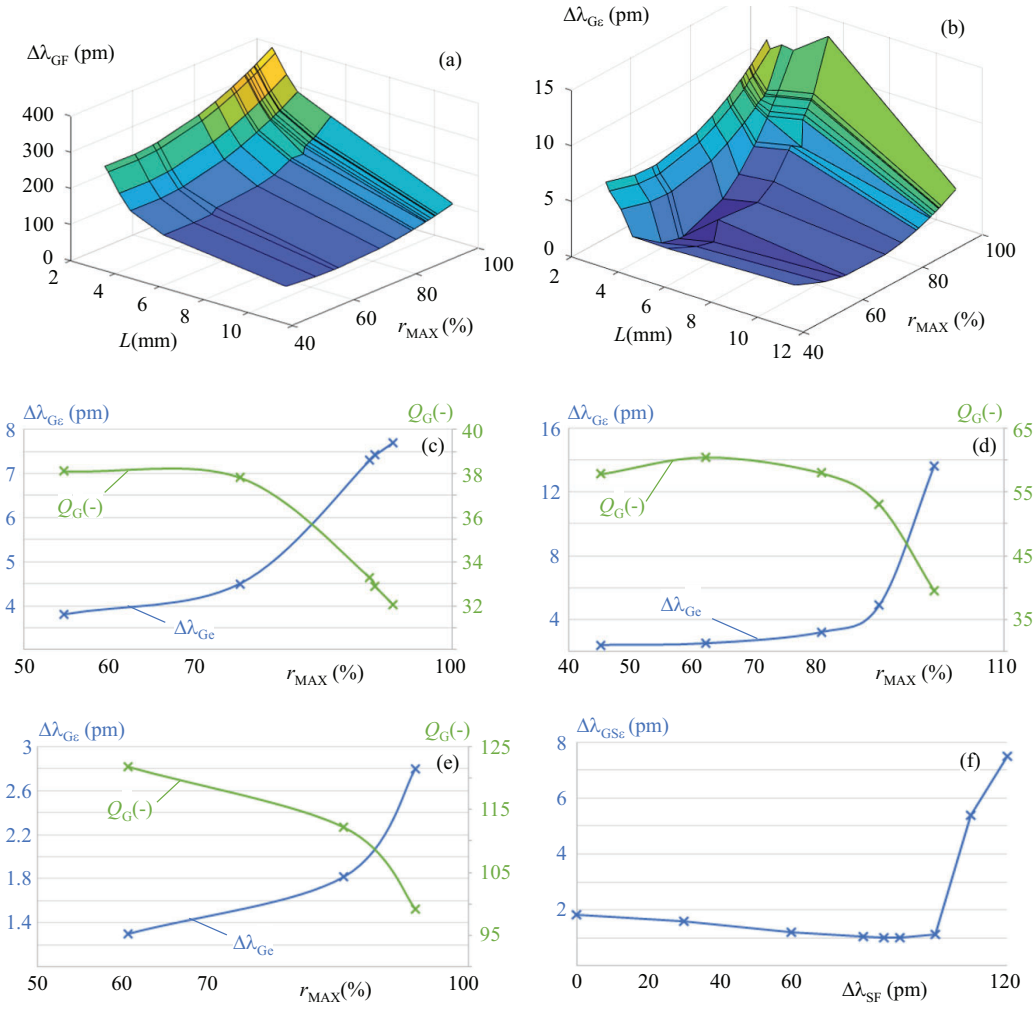

Fig. 8. (a) – Uniform rating reflectance linewidth versus grating length and reflectance, (b) – grating noise linewidth versus grating length and reflectance; grating quality factor and noise linewidth of the uniform grating versus grating reflectance for different grating lengths: (c) – 4.35 mm, (d) – 5.5 μm , and (e) – 11 mm; (f) – scanned noise linewidth $\Delta\lambda_{\mathrm{GS}\epsilon}$ of the uniform grating design No. 10-82, $\Delta\lambda_{\mathrm{GF}} = 82.5\,\mathrm{pm}$, scanned by the FWHM scanning spectrum linewidth $\Delta\lambda_{\mathrm{SF}}$

shows the scanned noise linewidth $\Delta\lambda_{\mathrm{GS}\epsilon}$ of the uniform grating No. 10-82 when scanned with the scanning spectrum linewidth varying from 0 to 120 pm. According to Fig. 5(b) while scanning with an ultra-narrow band source, the time signal $I_{\mathrm{m}}(t)$ practically copies the spectral grating reflectance.

$$I_{\mathrm{m}}(t) = I_{\mathrm{S0}} r_{\mathrm{G}}(k_\lambda t)\,, \tag{12}$$

where I_{S0} is the photoelectric response to the light intensity of the light source, and $r_G(k_\lambda t) = r_G(\lambda)$ is the spectral reflectance of the sensorial grating. This situation gives the scanned noise linewidth $\Delta\lambda_{\mathrm{GS}\epsilon}$ practically equal to the noise linewidth $\Delta\lambda_{\mathrm{G}\epsilon}$ of the scanned grating itself, see also Fig. 8(f). It is therefore interesting to see which design parameters influence the grating noise linewidth and which values of those parameters can provide us with the low noise linewidth value. The FBG design works [11,17,18,20,22] bring attention to the fact that the FWHM linewidth of the grating is grossly affected by the grating length and the reflectance. This relation is shown in the uniform grating design simulation, Fig. 8(a). The fact that the values of the noise linewidth of the gratings, as defined in Fig. 6, are, even for uniform gratings, not accurately proportional to the gratings FWHM linewidths depicts the graph of the experimental results in Fig. 8(b). There we can locate the area of maximal grating reflectance values and grating lengths to get the minimal noise linewidth. It is spread around the grating length $L = 10\,\mathrm{mm}$ and $r_{max} \cong 60\%$. Then, this way optimized uniform grating (design 10-60) gives the noise linewidth $\Delta\lambda_{Ge} = 1.3\,\mathrm{pm}$ and the mean error of the maximum reflectance wavelength measurement (8), $\sigma = 0.265\,\mathrm{pm}$, [22].

This is also supported by the graphs in Figs. 8(c)-(e), where one can see the behaviour of the measured grating noise linewidth and the calculated grating quality factor - as defined by (11) - for varying maximal reflectance. The graphs show the situation for three selected grating lengths within the most popular grating lengths interval. They support the conclusion that the suitable range of the maximal grating reflectance r_{max} for the scanning interrogation goes from 50 to 70%. As for the grating

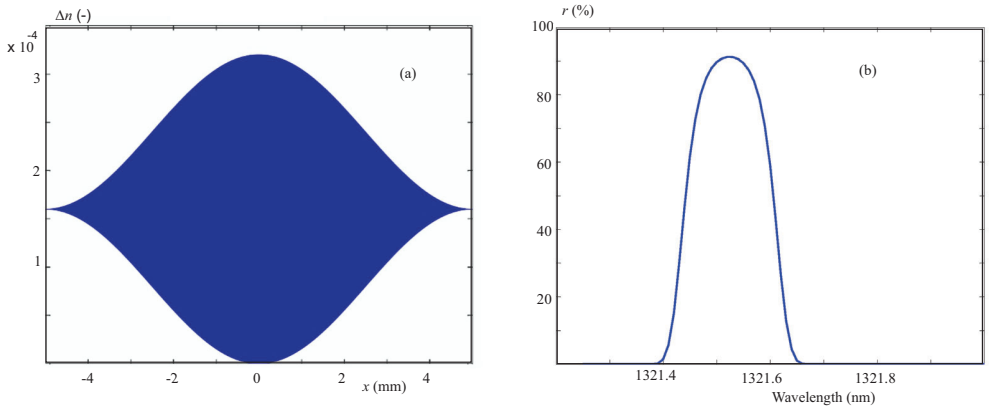

Fig. 9. (a) – Grating refractive index variation, and (b) – reflectance spectrum of the Design SAM-22 $\cos^2(\pi x/L)$ apodized grating, $L = 10\,\text{mm},\ \Delta\lambda_{\text{GF}} = 169\,\text{pm},\ r_{\max} = 91\,\%, \text{SLS} = -36\,\text{dB}$

length L, both simulations and the experiments show that the best results and the minimal values of the noise linewidth are seen with the lengts of the grating at the upper end of the applicable lengths interval, $L \geq 10\text{mm}$.

This was the situation of the grating spectrum scanned by the ultra narrow scaning spectrum. Scanning with a wider linewidth spectrum, such as the tunable FP filter spectrum with the scanning spectrum FWGM linewidth similar or comparable to the one of the grating itself, makes the situation more complex. The shape of spectral intensity of the scanning light $I_S(\lambda)$ has the FWHM linewidth $\Delta\lambda_{\text{SF}}$.

In general, this is different from the FWHM linewidth of $r_{\text{G}}(\lambda)$, and consequently, the linewidth and the shape of the the spectral corelation function $I_{\text{m}}(\lambda)$, see (4), is also different from $r_{\text{G}}(\lambda)$. Analyzing this effect we find the minimal value of the scanned grating noise linewidth $\Delta\lambda_{\text{GS}\epsilon}$ in the case of the interrogated grating and the scanning filter bear the equal values of $\Delta\lambda_{\text{F}}$

$$\Delta\lambda_{\text{SF}} = \Delta\lambda_{\text{GF}}\,. \tag{13}$$

The simulation of this situation for the uniform sensual grating, Design 10-82 with $L = 11\,\text{mm},\ r_{\max} = 85.6\,\%$, $\Delta\lambda_{\text{GF}} = 82.46\,\text{pm}$, is shown by the graph in Fig. 8(f). Here, the minimal value of scanned noise linewidth is $\Delta\lambda_{\text{GS}\epsilon} = 0.99\,\text{pm}$ and the RMS error $\sigma = 0.20\,\text{pm}$ for the case of scanning with the scanning filter linewidth $\Delta\lambda_{\text{SF}} = \Delta\lambda_{\text{GF}} = 82.5\,\text{pm}$. Let us point out that the optimal minimal scanned noise linewidth of 0.99 pm is nearly half of the scanned noise linewidth $\Delta\lambda_{\text{GS}\epsilon} = 1.82\,\text{pm}$ and RMS error $\sigma = 0.37\,\text{pm}$ of the same grating obtained if scanned with the ultra-narrowband tuneable source with $\Delta\lambda_{\text{SF}} \approx 0$.

The rules for the grating optimal reflectance and length to maximize the accuracy in measuring the spectral shift of the reflexivity of sensorial gratings, as shown in Fig. 8, are applicable fully to the design of the uniform gratings. Progress in the grating production technology gives some means to manipulate with the grating reflectivity spectrum and therefore some means to further improve the accuracy of the measurement. These means are in the modification of the grating structure of the longitudinal changes of the refractive index. This process, originally used to suppress the magnitude of the reflectance spectrum side lobes, got the name grating apodization. The simulation and the practical experiments have shown a good chance to decrease, by grating apodization process, the noise linewidth of the grating noticeably below the limit achievable by the uniform gratings.

5 Grating appodization

The grating structure with the amplitude of the longitudinal quasi-periodical change of the refractive index along the fiber axis modulated by a specific function is referred as an apodized grating. Several types of apodization with $\cos(x), \cos^2(x), \text{sinc}(x)$, Gaussian and other apodizing index amplitude functions found interesting applications. An important feature offered by the apodization is the grating reflectance spectrum side lobes suppression. Figure 9 shows this typical situation. The index apodization function used here is $\cos^2(\pi x/L)$ and the refractive index variation in the fibre core along the fibre x-axis is

$$\Delta n(x) = n_{\text{c}} + \Delta n_{\text{ph}}\Big(1 + \cos^2\frac{\pi x}{L}\sin\frac{2\pi x}{\Lambda_{\text{G}}}\Big)\,, \tag{14}$$

where n_{c} is the refractive index of the fibre core, Δn_{ph} is the photorefractive change of the fibre core refractive index.

The side lobes supression (SLS) achieved in this FBG design reaches $\text{SLS} = -36.8\,\text{dB}$, even with high reflexivity $r_{\max} = 91.0\,\%$. In comparison with the similar uniform grating (SAM-221) with the grating length $L = 10\,\text{mm}$ and the reflectance maximum $r_{\max} = 91.2\,\%$, the value of SLS is only 8.4 dB. The high side lobes supression of the apodized grating is a big advantage when using the grating as the narrowband filter, for example in the datacommunication applications. On the other hand, the full width half maximum linewidth of the apodized grating is rather large, $\Delta\lambda_{\text{GF}} = 169\,\text{pm}$, in contrast to the linewidth value $\Delta\lambda_{\text{GF}} = 100.6\,\text{pm}$ for the same length

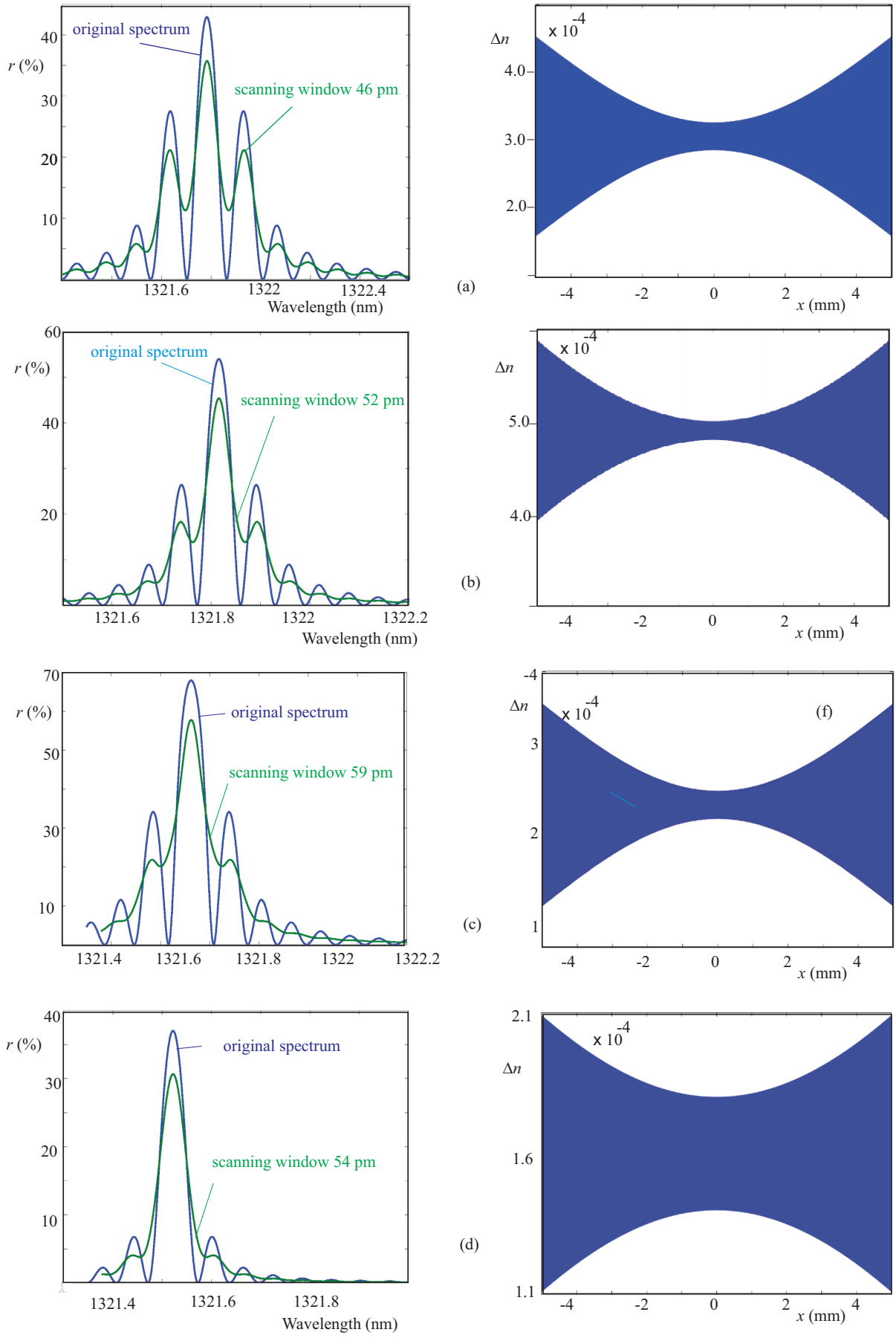

Fig. 10. Reflectance spectrum (left column) and the refractive index variation (right column) for: (a) – 2250-14, (b) – 2250-13, (c) – 2250-4, and (d) – 2250-15 apodized grating designs

Table 1. Features comparison of uniform (10-82, 10-60 and $\sin^2(x)$ apodized (2250-2257) gratings

	A	B	Δn_{ph}	$r_{\max}$	SLS	$\mathrm{SLS_s}$	$\Delta\lambda_{\mathrm{GF}}$	$\Delta\lambda_{\mathrm{G}\epsilon}$	$\Delta\lambda_{\mathrm{GS}\epsilon}$	σ
	-	-	$\times 10^{-4}$	%	dB	dB	pm	pm	pm	pm
10-82	0	1	0.625	85.6	8.75	24.4	82.46	1.82	0.99	0.20
10-60	0	1	0.4	60.5	10.8	>30	63.8	1.30	0.78	0.16
2250-14	0.35	0	3.5	43	1.93	4	46.0	0.912	0.501	0.102
2250-13	0.28	0.1	5	54	2.93	8.6	52.35	1.06	0.583	0.119
2250-4	0.5	0.15	2.2	67.7	3.01	13.4	58.47	1.16	0.638	0.130
2250-9	0.5	0.2	1.6	57.2	4.76	17.6	57.15	1.18	0.652	0.133
2250-15	0.3	0.2	1.8	37	7.38	17	53.9	1.23	0.676	0.138
2250-2	0.6	0.25	1.5	68.2	4.4	>30	62.65	1.26	0.693	0.141
2257	0.3	0.35	1.7	57.61	8.5	>30	64.76	1.27	0.698	0.142

and the same reflectivity uniform grating. Even though, this feature can be adored in the telecom filters, for the sensual purposes it is not welcomed.

The grating apodization technique should, in our expectation, narrow down the main peak of the grating reflectance spectrum, tolerating some increase of the side lobes in the spectrum. We have focussed our investigation on the apodization schemes based on the refractive index variation amplitude of $\cos(kx)$, $\sin(kx)$ and $\cos^2(kx)$, $\sin^2(kx)$ as these index profiles showed reasonable equality of the simulation and experimental results. Besides, these index profiles can be produced by the multi-exposition method that we use in our experimental setup. Expectedly, we have found the promising results using the apodization with the reverse apodization shapes than that one shown in Fig. 9.

We found the apodization function of the index variation amplitude based on the $\sin^2(A\pi x/L)$ amplitude function to give a grating with a narrow noise linewidth and a high grating quality factor [22] and still the multi-exposition method could be used for its implementation. The model of the fibre core refractive index variation along fibre was in this case

$$\Delta n(x) = n_{\mathrm{c}} + \Delta n_{\mathrm{ph}} \left[1 + \left([1-B] \sin^2 \frac{A\pi x}{L} + B \right) \sin \frac{2\pi x}{\Lambda_{\mathrm{G}}} \right]. \tag{15}$$

The three shape coefficients Δn_{ph}, A and B of this apodization allow to change the index variation amplitude profile widely. The criteria for optimization are to achieve a narrow noise linewidth, a narrow FWHM linewidth, high side lobe suppression and reasonable high reflectance. Some of the criteria are partially bound, some are mutually contradicting. The optimization is therefore a complex process, nevertheless, we found promissing results that have the potential for further refining. Figure 10. shows some results of the apodized grating design with index variation type according to (15). The gratings presented there have an active length of 10 mm. The upper plot, Fig. 10(a), represents the apodization grating design 2250-14 with the side lobes suppression of 1.93 dB. The (b) plot represents the apodization grating design 2250-13 with the side lobes suppression of 2.93 dB, further on, the (c) plot is for the design 2250-4 with the side lobe suppression of 3.01 dB, the lower design, Fig. 10(d) shows the grating 2250-15 with the side lobes suppression of 7.38dB. The blue lines in the spectrum charts are for the original apodized grating spectrum, the green lines are for the scanned spectrum. Here, the scanning always uses the optimized scanning spectrum linewidth, equal to the linewidth of the scanned apodized grating. Table 1 compares the sensorial grating features of the apodized gratings and uniform gratings of the same length. The results show the complex dependance of the noise linewidth $\Delta\lambda_{\mathrm{GSe}}$ to the grating reflectance and to the parameters A and B. Decreasing noise linewidth follows the decreasing B. The side lobes suppression (SLS) and scanned spectrum side lobes suppression (SLSs), which are also important spectral shape parameters, drop with decreasing B. Generally, the side lobes can bring troubles in identifying the main lobes of the spectra in case of serial connection of more sensing gratings to the scanning interogator. Therefore the compromise in the choice of the low noise linewidth and the low side lobe supression has to be accepted. Fortunately, the side lobe maxima decrease by scanning the spectra and the practice shows that the acceptable level of the resulting scanned spectrum side lobe suppression is 1:5 or 7 dB. That gives a bit limited choice of the exploitable designs, see Tab. 1.

6 Discussion

Our work was focused to the analysis of the factors influencing the accuracy of the scanning interrogation of the sensorial fibre Bragg gratings. The feasibility of the spectrum scanning interrogation method to get very fast reading of the grating reflectance spectrum and to obtain very fine resolution of the measured values has brought this method to the centre of our investigation. To utilize that high resolution, it was necessary to analyse the influence of the noise in the measurement. The analysis has

showed the importance of the specific features of the sensorial gratings to the measurement accuracy and errors.

We have formulated the influence of the reflectance of the grating, and then, we have focussed the work to the evaluation of the impact of the grating spectral width to the measurement accuracy. We have established the grating quality factor Q_{G} and grating noise linewidth $\Delta\lambda_{\mathrm{Ge}}$ for evaluation of the grating design suitability to the sensorial use. Our work has shown that, depending on the grating active length, there are optimal reflectances that shall give the best accuracy results in the scanning type of interrogation. Further, we have found that the spectrum scanning gives the best results when the scanning spectrum linewidth and the interrogated grating linewidth are equal. This optimal scanning gives nearly halved noise linewidth than the case of the scanning with the near to zero scanning spectral width. Increasing of the scanning spectrum linewidth above the value of the interrogated grating linewidth causes the rapid growth of the scanning noise linewidth and so the growth of the measuring errors.

The success of the grating apodization in forming the telecommunication class grating filters led us to check the potentiality of the grating apodization in sensing. The investigation of the grating apodization in the frame of this work was motivated by the aim to decrease the noise linewidth of the interrogated grating beyond the capabilities of the uniform grating design. Our work has proven the usefulness of the apodization as a way to further increase the accuracy of the fibre Bragg grating interrogation without the need to increase the grating active length. Within the possibilities of our grating manufacturing technology, we have found the prospective apodization profile $\sin^2(\pi x/L)$ that provides a decrease of the grating linewidth. However, that positive achievement is somewhat balanced by increasing the amplitudes of the side lobes in the reflectance spectrum of the interrogated grating. This can become a disturbing factor in spectrum scanning, especially in the case of scanning a chain of more gratings connected in series. Nevertheless, our work allows to conclude that the compromising apodization design of the grating and the optimal scanning can noticeably increase the measuring accuracy in the scanning interrogation of the sensing fibre Bragg gratings.

References

[1] L. Mescia and F. Prudenzano, "Advances on optical fiber sensors", *Fibers*, vol. 2, pp. 1-23, 2014.

[2] J. M. López-Higuera, L. R. Cobo, A. Q. Incera, and A. Cobo, "Fiber optic sensors in structural health monitoring", *Journal of Lightwave Technology*, vol. 29, no. 4, pp. 587-608, 2011.

[3] L. Schenato, "A Review of Distributed Fibre Optic Sensors for Geo-Hydrological Applications", *Applied Sciences*, vol. 7, no. 9, pp. 896, 2017.

[4] K. T. V. Grattan, and T. Sun, "Fiber optic sensor technology: An overview", *Sensors and Actuators A: Physical*, vol. 82, no. 1-3, pp. 40-61, 2000.

[5] J. M. López-Higuera, *Optical Sensors*, Universidad de Cantabria, Cantabria, Spain, 1998.

[6] J. M. López-Higuera, *Handbook of Optical Fibre Sensing Technology*, Wiley, 2002.

[7] J. Dakin and B. Culshaw, *Optical Fiber Sensors: Applications, Analysis and Future Trends*, Artech House, Boston, 1997.

[8] B. P. Pal, *Handbook of Optical Sensors*, CRC Press, https//www. routledgehandbooks.com/doi/10.1201/b17641-6. , 2014.

[9] F. Sales, F. Mota, L. Moura, G. Guimães, and A. Alexandria, "Applications of Fiber Bragg Grating Sensors in the Industry", *International Journal of Advanced Engineering Research and Science*, vol. 6, no. 12, pp. 238-250, 2019.

[10] J. K. Sahota, N. Gupta, and D. Dhawan, "Fiber Bragg grating sensors for monitoring of physical parameters: A comprehensive review", *Optical Engineering*, vol. 59, no. 6, pp. 1-35, 2020.

[11] L. K. Cheng, W. Vliegenhart, and T. Habisreuther, "Optical Fiber Grating based Technologies and Their Applications: from Nuclear Fusion to Medical", *Photonics Global Conference*, 5 pp. Singapore, 2012.

[12] T. K. Gangopadhyay, "Prospects for Fibre Bragg Gratings and Fabry-Perot Interferometers in fibre-optic vibration sensing", *Sensors and Actuators A: Physical*, vol. 113, no. 1, pp. 20-38, 2004.

[13] M. S. Ferreira, M. Becker, H. Bartelt, P. Mergo, J. L. Santos, and O. Frazão, "A vibration sensor based on a distributed Bragg reflector fibre laser", *Laser Physics Letters*, vol. 10, no. 9, 095102, 2013.

[14] M. S. Ferreira, J. Bierlich, M. Becker, K. Schuster, J. L. Santos, and O. Frazão, "Ultra-high sensitive strain sensor based on post-processed optical fiber Bragg grating", *Fibers*, vol. 2, pp. 142-149, 2014.

[15] F. Berghmans et al., "Microstructured optical fiber Bragg grating sensors for structural health monitoring applications,", *7th European Workshop on Structural Health Monitoring*, Nantes, France pp. 962-969, 2014.

[16] W. W. Morey, G. Meltz, and W. H. Glenn, "Fiber Optic Grating Sensors", *Proc. SPIE 1169, Fiber Optic and Laser Sensors*, VIIhttps://doi.org/10.1117/12.963022 , 1990.

[17] K. O. Hill and G. Meltz, "Fiber Bragg Grating Technology Fundamentals and Overview", *Journal of Lightwave Technology*, vol. 15, no. 8, pp. 1263-1276, 1997.

[18] Z. Zhou, T. W. Graver, L. Hsu and J. Ou, "Techniques of advanced FBG sensors: Fabrication, demodulation, encapsulation, and their application in the structural health monitoring of bridges", *Pacific Science Review*, vol. 5, pp. 116-121, 2003.

[19] K. Zhou, M. Dubov, C. Mou, L. Zhang, V. K. Mezentsev, and I. Bennion, "Line-by-line fiber Bragg grating made by femtosecond Laser", *IEEE Photonics Technology Letters*, vol. 22, no. 16, pp. 1190-1192, 2010.

[20] B. Kawasaki, K. O. Hill, D. C. Johnson, and Y. Fujii, "Narrow-band Bragg reflectors in optical fibers", *Optics Letters*, vol. 3, no. 2, pp. 66-68, 1978.

[21] H. D. Lee, G. H. Kim, T. J. Eom, M. Y. Jeong, and C.-S. Kim, "Linearized Wavelength Interrogation System of Fiber Bragg Grating Strain Sensor Based on Wavelength-Swept Active Mode Locking Fiber Laser", *Journal of Lightwave Technology,*, vol. 33, no. 12., pp. 2617-2622, 2015.

[22] F. Urban Jr, R. Helan, and F. Urban Sr., "Sensoric Fiber Bragg Grating design for scanning interrogation", *Proceedings of the 8th International Conference on Sensors and Electronic Instrumental*, Advances SEIA, pp. 38-44, 2022.

Received 24 January 2023